Original Article

NICORANDIL MITIGATES ARTHROGENIC CONTRACTURE INDUCED BY KNEE JOINT EXTENSION IMMOBILIZATION IN RATS: INTERFERENCE WITH RHOA/ROCK SIGNALING AND TGF-β1/SMAD PATHWAY

X.M. Li[1,2,§], K. Wang[1,2,§], M. Liu[1,2,3], Q.B. Zhang[1,2] and Y. Zhou[1,2,*]

[1]Department of Rehabilitation Medicine, The Second Affiliated Hospital of Anhui Medical University, 230601 Hefei, Anhui, China
[2]Research Center for Translational Medicine, The Second Affiliated Hospital of Anhui Medical University, 230601 Hefei, Anhui, China
[3]Department of Rehabilitation Medicine, The First Affiliated Hospital of University of Science and Technology of China, 230022 Hefei, Anhui, China
[§]These authors contributed equally

Abstract

Objective: Prolonged immobilization often results in myogenic and arthrogenic contractures, with capsular fibrosis being the critical aspect of the latter. This study aimed to determine whether nicorandil can mitigate joint contracture and fibrosis by inhibiting the RhoA/ROCK signaling pathway, thereby affecting the TGF-β1/Smad signaling pathway. **Materials and Methods**: This study used a rat model of knee extensor joint immobilization to assess the impact of nicorandil on arthrogenic contracture and joint capsule fibrosis. Sixty Sprague–Dawley rats were divided into control, immobilization, and nicorandil treatment groups with varying durations of immobilization. The extent of arthrogenic contracture was assessed using joint mobility metrics, while joint capsule fibrosis was quantified using Masson staining, α-SMA immunohistochemistry, and H&E staining. The protein expression levels of the TGF-β1/Smad and RhoA/ROCK signaling pathways were analyzed by western blotting. Additionally, lysophosphatidic acid (LPA), a specific ROCK activator, was used to further investigate the involvement of RhoA/ROCK signaling in TGF-β1/Smad pathway modulation. **Results**: This study revealed a positive correlation between the duration of immobilization and the severity of arthrogenic contracture, joint capsule fibrosis, and inflammatory infiltration. Nicorandil administration effectively reduced these immobilization-induced changes and concurrently inhibited the activation of TGF-β1/Smad and RhoA/ROCK signaling pathways. Application of LPA counteracted the inhibitory effects of nicorandil on these pathways. **Conclusion**: Nicorandil significantly alleviated arthrogenic contracture and joint capsule fibrosis resulting from knee extension immobilization. The underlying mechanism appears to involve inhibition of the TGF-β1/Smad signaling pathway, mediated by RhoA/ROCK signaling pathway suppression.

Keywords: Nicorandil, arthrogenic contracture, fibrosis, TGF-β1/Smad signaling pathway, RhoA/ROCK signaling pathway.

***Address for correspondence**: Yun Zhou, MD, PhD, Department of Rehabilitation Medicine, The Second Affiliated Hospital of Anhui Medical University, No.678 Furong Road, Economic and Technological Development Zone, Hefei 230601, China. Telephone number: +8618715154895; E-mail: zhouyunanhui@sina.com

Introduction

Regardless of whether the injury is sports-related or traumatic, the knee is often treated according to the POLICE principle: Protest, Optimal Loading, Ice, Compression, and Elevation. Prolonged braking of the knee is one of the most important causes of joint contractures. In the early stages of immobilization, myogenic contractures occur first, followed by arthrogenic contractures, which are contractures of the joint capsule, articular cartilage, ligaments, and other tissues (Zhang *et al*., 2023). It is usually more difficult to intervene effectively in arthrogenic contractures. The pathological mechanism of arthrogenic contracture involves fibrosis of the joint capsule. Fibrosis has been described as excessive proliferation of fibroblasts and myofibroblasts, deposition of extracellular matrix, increased content of collagen fibers, and in some studies, the presence of lymphocyte infiltration (Huang *et al*., 2021).

Myofibroblasts are activated after tissue injury. These cells produce an extracellular matrix that facilitates repair. If they do not undergo apoptosis after successful repair, myofibroblasts persistently produce excess matrix, leading to extensive scarring and fibrosis. Tissue fibrosis can be effectively alleviated by inhibiting myofibroblast activation

(Yu *et al*., 2021). Therefore, chronic fibrotic lesions are characterized by the persistence of myofibroblasts. Rho-GTPase and ROCK are major signaling molecules in the RhoA/ROCK pathway. ROCK activation leads to the formation of F-actin stress fibres, decreasing the abundance of G-actin and exposing the nuclear localisation sequence of Myocardin-Related Transcription Factor (MRTF). This leads to nuclear accumulation of MRTF, where it can bind to serum response factor (SRF) and induce gene expression (Tsou *et al*., 2014). Whereas multiple target genes of MRTF/SRF are known drivers of fibrosis (Hanna *et al*., 2009; Luchsinger *et al*., 2011; Mack *et al*., 2001). Studies have shown that the absence of ROCK2 in cardiac fibroblasts leads to cardiac hypertrophy and reduced fibrosis (Shimizu *et al*., 2017).

ROCK1 was shown to play a more important profibrotic role than ROCK2 in knockout ROCK1 and haploid ROCK1 mic (Sunamura *et al*., 2018). Previous literatures had shown that inhibition of the Rhoa/Rock signalling pathway can attenuate pulmonary and renal fibrosis (Jiang *et al*., 2012; Komers, 2013). Lysophosphatidic acid (LPA) promotes tissue fibrosis by activating TGFβR1 via a RhoA/ROCK-dependent pathway (Zhou *et al*., 2021), leading to the release of TGF-β and subsequent activation of downstream signalling pathways. It has been demonstrated that the expression levels of TGF-β1, RhoA, and ROCK1 are all significantly increased in rats with uterine adhesions and decreased in human Wharton's glial MSCs. This also confirms that the RhoA/ROCK signaling pathway is involved in fibrosis of uterine epithelial cells (Li *et al*., 2021).

Nicorandil (2-nicotinamideethyl nitrate) is an ATP-sensitive potassium channel opener, and it has been proven safe in animal experiments (Garnier-Raveaud *et al*., 2002; Lee *et al*., 2008). In rats with myocardial infarction, Lee *et al*. (Lee *et al*., 2008) found that nicorandil significantly slowed cardiomyocyte hypertrophy and the area of cardiac fibrosis. In addition to inhibiting myocardial fibrosis, the antifibrotic effects of nicorandil have been discovered in other tissues, such as lung tissues (El-Kashef, 2018; Kseibati *et al*., 2020) and hepatic tissues (Abdel-Sattar *et al*., 2020; Mohamed *et al*., 2018). The molecular mechanism by which nicorandil attenuates fibrosis has not been elucidated. In a rat model of myocardial infarction, nicorandil inhibited RhoA translocation and inactivated ROCK, and it enhanced the activation of M2 macrophages, which reduced the infiltration of myofibroblasts in the infarcted area and collagen accumulation (Lee *et al*., 2018). Given the functions of nicorandil established in previous studies, we hypothesized that nicorandil treatment effectively attenuates and slows the progression of arthrogenic fibrosis by inhibiting the RhoA/ROCK signaling pathway and modulating the TGF-β1/Smad signaling pathway.

Methods

Animals and Grouping

Sixty skeletally mature male Sprague–Dawley rats (Experimental Animal Center of Anhui Medical University, Hefei, China, 3 months old, weighing 250-300 g) were used in this experiment. The rats were housed in standard cages (room temperature 24 °C-25 °C, 12 h light/dark cycle) for 2 weeks, with four rats per cage, and the rats had free access to food and water. The experimental protocol was divided into two parts. In the first part, test a, 42 rats were randomly assigned to a control group (group C, rats without any intervention, n = 6), a immobilization group (groups I-1w(a), I-2w(a), and I-4w(a) for 1, 2, and 4 weeks of immobilization, respectively, with saline gavage during the immobilization period, n = 6), and a nicorandil-treated group (groups N-1w(a), N-2w(a), and N-4w(a), respectively, were immobilized for 1, 2, and 4 weeks of nicorandil gavage during immobilization, n = 6) using random number table method. In the second part, test b, 18 rats were randomly assigned to a immobilization group (I-4w(b) group, 4 weeks of immobilization; n = 6), a nicorandil-treated group (N-4w(b) group, using nicorandil by gavage for 4 weeks of immobilization, n = 6), or a nicorandil-treated combined LPA group (N+LPA group, using nicorandil by gavage and concurrently injecting LPA intraperitoneally for 4 weeks of immobilization; n = 6) using random number table method (Fig. 1**a,b**).

For the experimental procedure, the rats were anesthetized in batches by intraperitoneal injection of 40 mg/kg sodium pentobarbital. Subsequently, the left knee joint of the rats was placed in a fully extended position and immobilized using the support method previously used in the experimental group (Zhou *et al*., 2023) (Patent No. 02120470158.0) (Fig. 2**A**). The immobilization time was determined as indicated in the previous grouping instructions. The rats were observed daily for loosening of the immobilization device and health status to make timely adjustments. During the immobilization period, the N-1w(a), N-2w(a), N-4w(a), and N-4w(b) groups were subjected to nicorandil gavage at 3 mg/kg once a day. For comparison, groups I-1w(a), I-2w(a), I-4w(a), and I-4w(b) were subjected to immobilization for the corresponding period, and saline gavage was used. To further verify the involvement of RhoA/ROCK in the fibrotic process, rats in the N+LPA group received LPA, a ROCK activator, 40 µg/kg intraperitoneally (Davies *et al*., 2017) via once-daily gavage of nicorandil (3 mg/kg) (Mohamed *et al*., 2018).

Measurement of Joint Contracture

Rats in each group were euthanized by intraperitoneal injection of 10 % chloral hydrate 400 mg/kg after an adequate time of immobilization. In test a, the left hind limb of the rats was disarticulated and completely excised from the left hip joint. As in previous studies (Zhou *et al*., 2023), we measured knee range of motion (ROM) at this point using a knee measurement tool (Patent No. ZL202120996643.1).

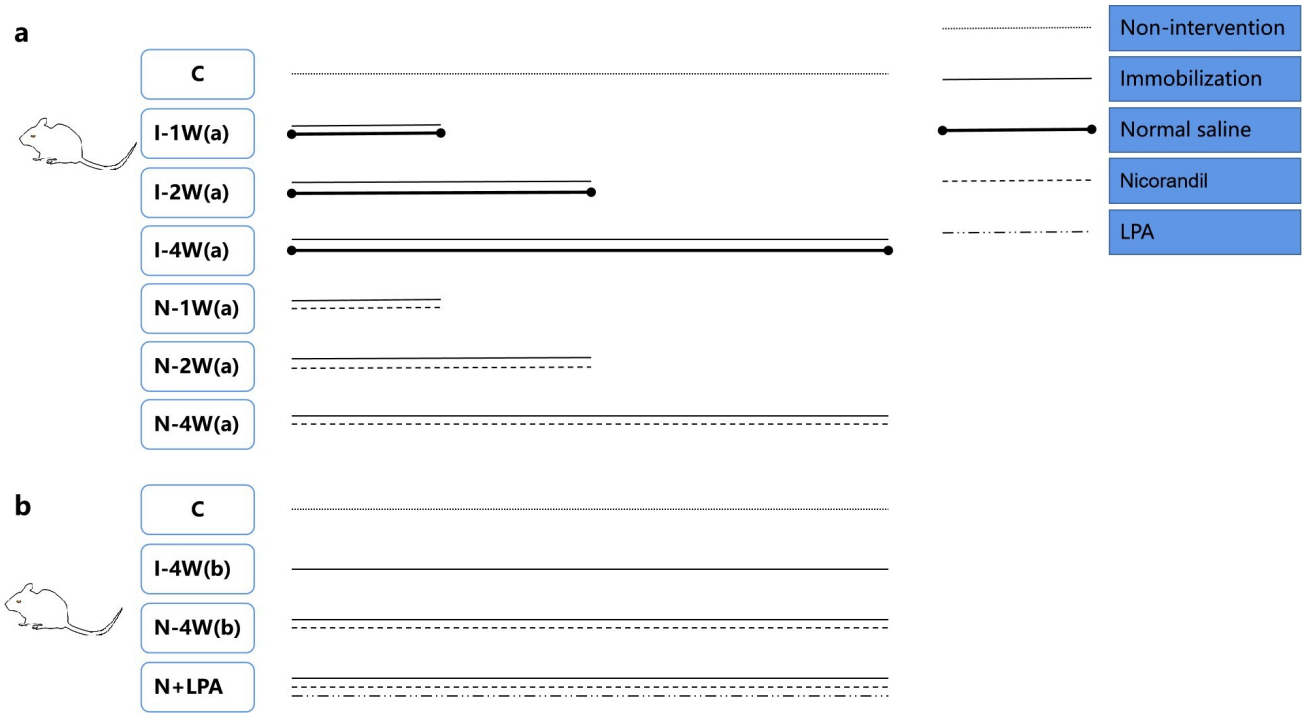

Fig. 1. Experimental Groups and Intervention Methods. (**a**) Design of trial a in this study. (**b**) Design of test b in this study.

Subsequently, the muscles around the knee joint were excised, the intact knee capsule structure was preserved, and ROM was measured again. Two study members without knowledge of subgroups conduct the measurements of ROM. The degree of knee contracture was defined using the following formula (Fig. 2**B,C**):

Total contracture angle = (control knee) pre-myotomy ROM – (contracted knee) pre-myotomy ROM.

Arthrogenic contracture angle = (control knee) post-myotomy ROM – (contracted knee) post-myotomy ROM.

Tissue Preparation

At the end of the experimental cycle, the rats were euthanized. The excised anterior capsule of the rat knee was cut into small portions and used to prepare the joint capsule homogenates and histopathological sections. A portion of the anterior joint capsule tissue was homogenized at 1000 ×g, centrifuged at 4 °C for 15 min, and the supernatant was collected and stored at - 80 °C for determination of TGF-β1, RhoA, ROCK1, and p-MLC. Some of the anterior joint capsule samples were immediately fixed in 10% neutral buffered formalin solution in saline for 24 h. They were rinsed with tap water and then dehydrated with graded concentrations of ethanol (50 % ~ 100 %). The specimens were cleared in xylene and embedded in paraffin in a hot air oven at 56 °C for 24 h. Waxy paraffin nectar tissue blocks were prepared using a slide slicer and cut to a thickness of 4-5 μm.

Masson Staining

The degree of joint capsule fibrosis was assessed using Masson staining. Staining was performed using a Masson Staining Solution Kit (Servicebio, Wuhan, Hubei, China). Paraffin sections were dewaxed, dehydrated, immersed in Masson A solution overnight, rinsed under running tap water, placed in an equal mixture of Masson B and Masson C solutions, washed with water, and then differentiated using a differentiation solution. Massons D and E were used for staining and rinsing, respectively. Masson F was used for staining. The sections were dehydrated with anhydrous ethanol, made transparent with xylene for 5 min, and sealed with neutral gum. The sections were observed under a microscope (BX43F; Olympus, Tokyo 163-0914, Japan) at 400× magnification, and six fields of view were randomly selected and photographed. Collagen deposition was expressed as a percentage of the blue area and analyzed using Image-Pro Plus 6.0 (Media Cybernetics, Rockville, MD, USA).

Immunohistochemistry

The degree of joint capsule fibrosis was evaluated using immunohistochemistry. The paraffin sections were dewaxed and dehydrated for antigenic autoclave repair. Next, 2 L of citrate repair solution (Zsbio, Beijing, China) was prepared, and the sections were placed in an autoclave and boiled for 2 min for hot repair. The sections were incubated for 20 min at room temperature by drawing a circle around the tissue with an immunohistochemistry pen and adding 3 % H_2O_2 dropwise to the tissue. Sections were rinsed three

A

D

Grouping	Quantity	Degree of contracture(°)	
		Total contracture	Arthrogenic contracture
Group C	6	0±0	0±0
Group I-1W(a)	6	25.42±3.03^{a}	9.64±1.4^{a}
Group N-1W(a)	6	19.48±1.46^{a*}	6.42±0.67^{a*}
Group I-2W(a)	6	50.67±3.07$^{ab'}$	20.42±1.49$^{ab'}$
Group N-2W(a)	6	43.75±2.14$^{ab\#}$	16.06±1.82$^{ab\#}$
Group I-4W(a)	6	77.44±17.8$^{ab'c'}$	47.94±2.86$^{ab'c'}$
Group N-4W(a)	6	68.63±2.39$^{abca'}$	41.36±2.64$^{abca'}$

B

C

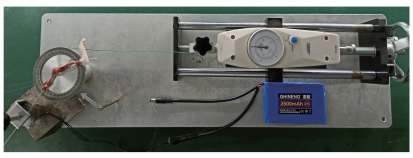

E

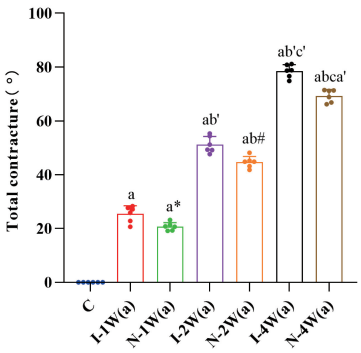

F

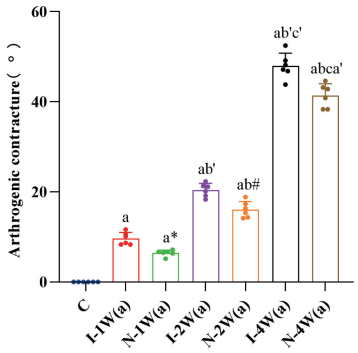

Fig. 2. Animal model and joint mobility of rats. (**A**) Animal model. The left knee joint of the rat was immobilized in full extension using a shaped aluminum splint. (**B**) The left hind limb of each rat was immobilized (before muscle incision) on the arthrokinesis meter. The handle was then turned (maintaining a constant torque of 0.053 Nm) and the range of motion of the left knee joint before and after myotomy was read from the scale on the dial. (**C**) The left hind limb of each rat was immobilized (after myotomy) on the arthrokinematic measuring instrument. The handle was then turned (maintaining a constant torque of 0.053 Nm) and the range of motion of the left knee joint before and after myotomy was read from the scale on the dial. (**D**) Total joint range of motion and arthrogenic contracture of rats in each group. (**E**) Comparison of total joint mobility of rats in each group. (**F**) Comparison of arthrogenic contracture in rats in each group. ($^{a}p < 0.05$ vs. group C, $^{b}p < 0.05$ vs. group N-1w(a), $^{c}p < 0.05$ vs. group N-2w(a), $^{b'}p < 0.05$ vs. group I-1w(a), $^{c'}p < 0.05$ vs. group I-2w(a), $^{*}p < 0.05$ vs. group I-1w(a), $^{\#}p < 0.05$ vs. group I-2w(a), $^{a'}p < 0.05$ vs. I-4w(a) group).

times using PBS, after which the sections were shaken dry and incubated overnight at 4 °C with rabbit anti-α-SMA antibody (1:100; Affinity Biosciences). The sections were washed and incubated with secondary antibodies at 37 °C for 30 min. DAB colorant was added, the color development time was controlled under a microscope (with positive termination of color development), and the sections were rinsed in distilled water and stained with hematoxylin and lithium carbonate. It was then made transparent with xylene and sealed with a neutral adhesive. Each section was observed under a microscope (BX43F; OLYMPUS, Tokyo 163-0914, Japan) at 400× magnification, and five fields of view were randomly selected and photographed. Finally, the percentage of positive cells in the entire field of view was calculated for each picture using Image-Pro Plus 6.0 software as an indicator of their positive expression.

H&E Staining

The total cell count and inflammatory cell infiltration of the joint capsule were assessed by H&E staining. Paraffin sections were deparaffinized and dehydrated using hematoxylin (Baso, Zhuhai, Guangdong, China) staining solution for 3-5 minutes and blued using dilute lithium carbonate for 30 s. The sections were dehydrated with ethanol and stained using eosin staining solution (Baso, Zhuhai, Guangdong, China) for 10-30 seconds. It was made transparent using xylene and sealed with neutral gum. Observations were performed under a microscope (BX43F; Olympus, Tokyo 163-0914, Japan) at 400× magnification, and six fields of view were randomly selected and photographed. The cells in the joint capsule consist mainly of myofibroblasts and inflammatory cells, which are distinguished by morphological identification. We counted these different types of cells together to briefly show the inflam-

mation and fibrosis of the joint capsule, and the cells were analyzed using Image-Pro Plus 6.0.

Western Blotting

The protein expression levels of TGF-β1, Smad2/3, p-Smad2/3, α-SMA, Collagen I, RhoA, ROCK1, and p-MLC were analyzed using western blotting. The supernatant of the prepared joint capsule homogenate was used to determine the protein concentration using a bicinchoninic acid (BCA) protein quantification kit (Beyotime, Shanghai, China). Next, equal amounts of protein from each pair of samples were separated by SDS–PAGE on a 10 % polyacrylamide gel and electrotransferred to a polyvinylidene difluoride microporous membrane, which was then blocked in 5 % skim milk before being dissolved in TBST and incubated for 2 h at room temperature. Membranes were incubated overnight at 4 °C with various primary antibodies. On the second day, the membranes were incubated with secondary antibody for 45 min at room temperature and then washed three times with TBST solution. Finally, ECL chemiluminescent droplets were added to the target band, and the signal was detected with a digital imaging device. The density of each band was quantified using Image-Pro Plus software (version 6.0). TGF-β1, Smad2/3, p-Smad2/3, α-SMA, Collagen I, RhoA, ROCK1, and p-MLC proteins were calculated by comparing them with the amount of GAPDH as a loading control.

Data Analysis

The results are expressed as the mean $\pm$ standard deviation. Statistical analyses were performed using IBM SPSS Statistics version 26 (IBM Corp., Armonk, NY, USA). In test a, One-way ANOVA was used for within-group comparisons in groups N(N-1w(a), N-2w(a), and N-4w(a)) or I(I-1w(a), I-2w(a), and I-4w(a)). *T*-test was used to compare the immobilization groups and nicorandil-treated groups with the control group. At the same time point during immobilization, *T*-test were used for intergroup comparisons between the groups N and groups I. For test b, between-group comparisons were performed using an unpaired *t* test. Statistical significance was set at $p < 0.05$.

Results

None of the rats died during the immobilization period. No prolonged edema or acute inflammation was observed in the hind limbs of the rats.

Arthrogenic Contracture

The results of test a showed that the total degree of contracture and arthrogenic contracture increased with increasing immobilization time in groups N(a) and I(a) ($p < 0.05$) (Fig. 2**D-F**). At the same time point, there was a significant increase in arthrogenic contracture in group I(a) compared to group N(a) ($p < 0.05$, Fig. 2**F**). Thus, nicorandil had a good therapeutic effect on immobilization-induced arthrogenic contractures.

H&E Staining of the Joint Capsule

To investigate the anti-inflammatory effect of nicorandil, we performed H&E staining of the joint capsule. The results of H&E staining and quantitative analysis showed that the total cell number and inflammatory cell infiltration tended to increase with increasing immobilization time in both group I(a) and group N(a) ($p < 0.05$). In test a, at the same time point, the total cell count and inflammatory cell infiltration were significantly reduced in group N(a) compared to those in group I(a) ($p < 0.05$) (Fig. 3**A,B**). These results suggest that nicorandil attenuates the immobilization-induced inflammatory response.

Joint Capsule Fibrosis

To study the effect of nicorandil on fibrosis of the joint capsule, we performed Masson staining and western blotting for collagen I on the joint capsule. As shown in the figure, the collagen area and collagen I level tended to increase significantly in both group I(a) and group N(a) as the immobilization time increased ($p < 0.05$). During the 4-week immobilization period, the collagen area and collagen I increased to different degrees in both group I(a) and group N(a). At the same time point, the increased area of collagen and elevated collagen I were more obvious in group I(a) than in group N(a) ($p < 0.05$) (Fig. 4**A,B**, Fig. 5**A,C**). To further determine the severity of fibroblast differentiation into myofibroblasts in the joint capsule, we examined the immunohistochemical and protein levels of α-SMA in the joint capsule. As shown, α-SMA expression tended to increase significantly in both the I(a) and N(a) groups with increasing immobilization time ($p < 0.05$). During the 4-week immobilization duration, the percentage of cells expressing α-SMA increased to different degrees in both group I(a) and group N(a); at the same time point, the percentage of cells expressing α-SMA was more pronounced in group I(a) than in group N(a) ($p < 0.05$, Fig. 6**A,B**). The results of the WB assay of α-SMA protein in the rat joint capsule showed the same results as above (Fig. 5**A,B**). In conclusion, the oral administration of nicorandil has a protective effect against immobilization-induced fibrosis in rats.

The Expression Level of the TGF-β1/Smad Signaling Pathway

The TGF-β1/Smad signaling pathway includes TGF-β1, Smad2/3, p-Smad2/3, collagen I, and α-SMA. The expression levels were increased in both the N-4w(b) and I-4w(b) groups compared to the control group C ($p < 0.05$) (Fig. 5**D-H**). But the expression level of the TGF-β1/Smad signaling pathway was significantly reduced in the N-4w(b) group compared with the I-4w(b) group ($p < 0.05$) (Fig. 5**D-H**). However, the TGF-β1/Smad signaling pathway expression level was significantly higher in the N+LPA group

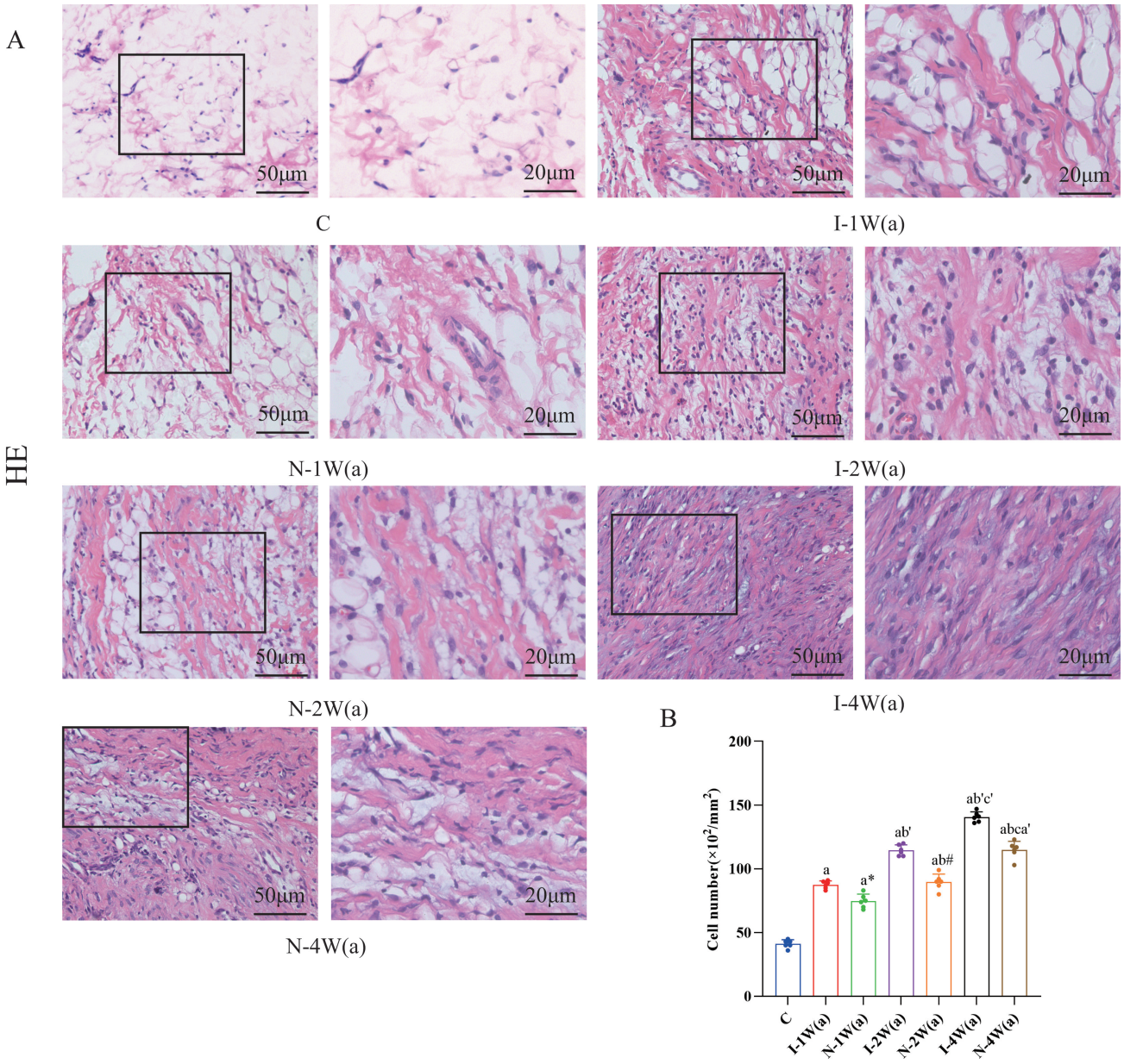

Fig. 3. H&E staining. (**A**) Results of H&E staining of the joint capsule. The scale bars indicate 50 μm (left panels) and 20 μm (right panels). (**B**) Quantitative analysis of total cell number in each group. Data are expressed as mean ± standard deviation. ($^{a}p < 0.05$ vs. group C, $^{b}p < 0.05$ vs. group N-1w(a), $^{c}p < 0.05$ vs. group N-2w(a), $^{b'}p < 0.05$ vs. group I-1w(a), $^{c'}p < 0.05$ vs. group I-2w(a), $^{*}p < 0.05$ vs. group I-1w(a), $^{\#}p < 0.05$ vs. group I-2w(a), $^{a'}p < 0.05$ vs. I-4w(a) group).

than in the N-4w(b) group. In summary, nicorandil inhibited the protein expression level of the TGF-β1/Smad signaling pathway in the joint capsule to a certain extent, whereas LPA counteracted the inhibitory effect on the TGF-β1/Smad signaling pathway in the joint capsule.

The Expression Level of the RhoA/ROCK1 Signaling Pathway

The RhoA/ROCK signaling pathway includes the RhoA, ROCK1, and p-MLC proteins. Total RhoA protein did not show significant changes in any of the groups (Fig. 5**D,J**). The expression levels of ROCK1 and p-MLC proteins were increased in both the N-4w(b) and I-4w(b) groups compared with the control group C ($p < 0.05$) (Fig. 5**D,I,K**). However, ROCK1 and p-MLC protein expression levels were suppressed in the N-4w(b) group compared with those in the I-4w(b) group ($p < 0.05$) (Fig. 5**D,I,K**). This indicated that nicorandil inhibited activation of the RhoA/ROCK signaling pathway in the joint capsule during immobilization. However, ROCK1 and p-MLC proteins were significantly higher in the N+LPA group than in the N-4w(b) group ($p < 0.05$) (Fig. 5**D,I,K**). Thus, LPA effectively reversed RhoA/ROCK activation induced by nicorandil in the joint capsule during immobilization.

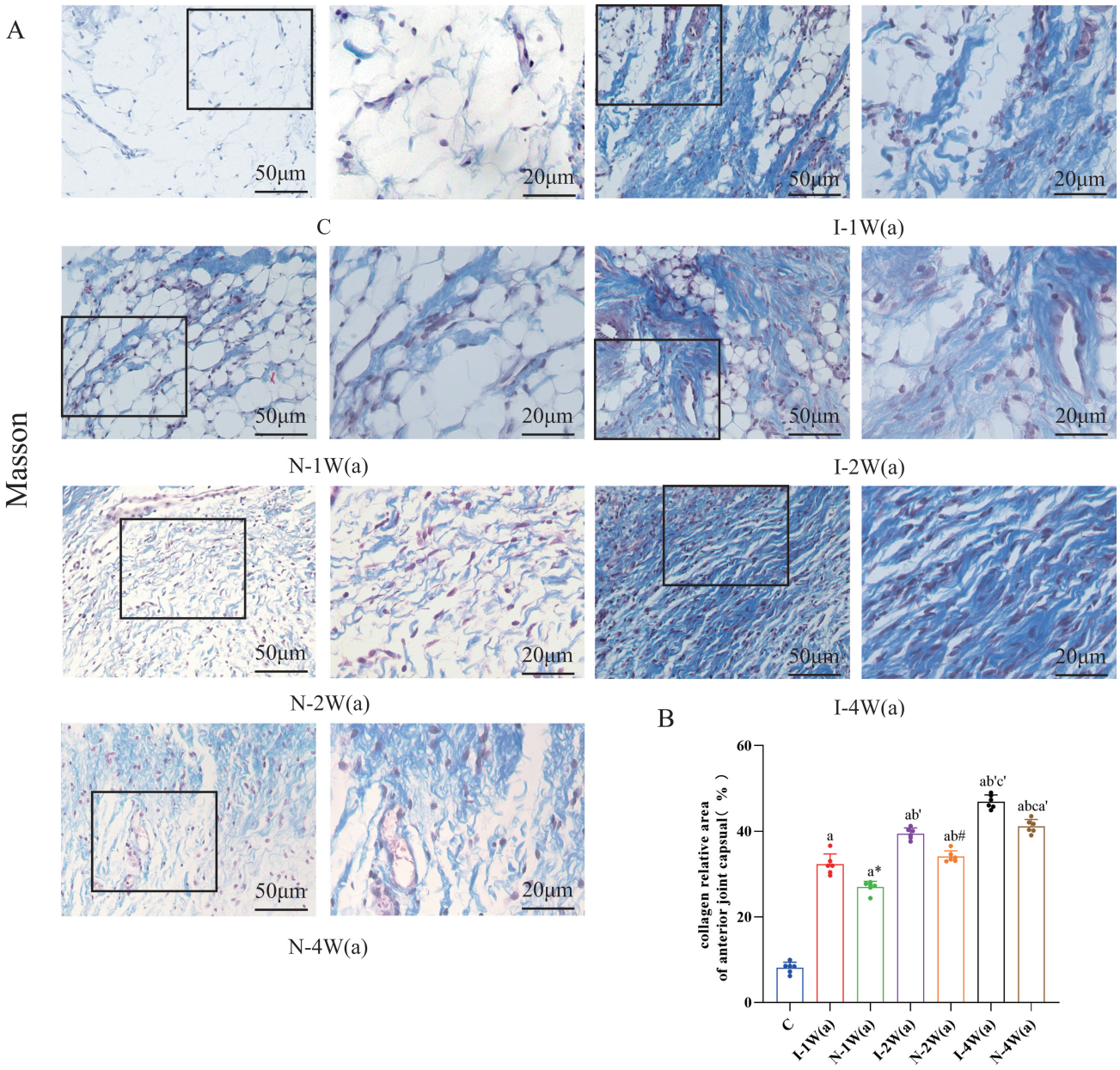

Fig. 4. Masson staining. (**A**) Masson staining results of the joint capsule, field of view. The scale bars indicate 50 μm (left panels) and 20 μm (right panels). (**B**) Quantitative analysis of the percentage of collagen deposition (blue area) in each group. Data are expressed as mean ± standard deviation. ($^{a}p < 0.05$ vs. group C, $^{b}p < 0.05$ vs. group N-1w(a), $^{c}p < 0.05$ vs. group N-2w(a), $^{b'}p < 0.05$ vs. group I-1w(a), $^{c'}p < 0.05$ vs. group I-2w(a), $^{*}p < 0.05$ vs. group I-1w(a), $^{\#}p < 0.05$ vs. group I-2w(a), $^{a'}p < 0.05$ vs. I-4w(a) group).

Discussion

In the present study, we investigated the effect of nicorandil on arthrogenic contracture induced by immobilization of the rat knee at several levels, including morphological, histological, and molecular levels. Recent studies have shown that nicorandil inhibits TGFβ1-induced collagen secretion and ECM deposition during chronic fibrosis in a variety of tissues (Abdel-Aziz *et al*., 2023; El-Kashef, 2018; Kseibati *et al*., 2020). Here, we demonstrated that nicorandil can inhibit arthrofibrosis via the RhoA/ROCK-mediated TGF-β1/Smad signaling pathway during knee immobilization (Fig. 7), suggesting that nicorandil has therapeutic potential as a new therapeutic agent for arthrogenic contractures.

Joint immobilization is often unavoidable as the most common treatment after an injury occurs. Immobilization usually takes one month or more after a fracture or ligament injury. During the first period of immobilization, atrophy and fibrosis of the periarticular muscles occur, followed by ligament shortening, collagenous hyperplasia and fibrosis (Huang *et al*., 2021; Zhou *et al*., 2023). Previous studies have confirmed that 4 weeks of free movement after the re-

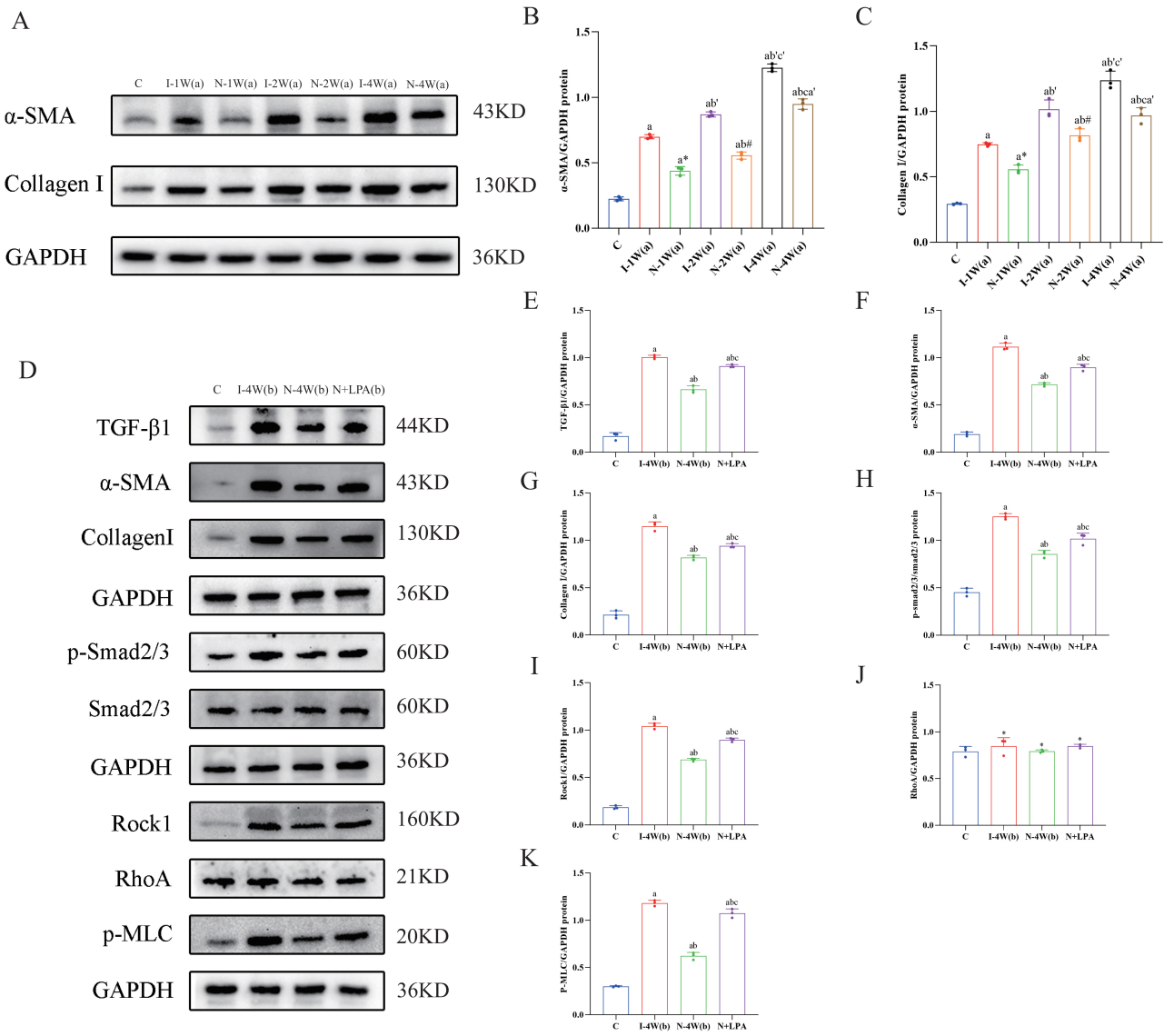

Fig. 5. Western Blot. (**A**) Expression of α-SMA and collagen I of the joint capsule were examined by Western blotting. (**B,C**) The α-SMA/GAPDH and Collagen I/GAPDH of the joint capsule in each group. Data are expressed as mean ± standard deviation. ($^{a}p < 0.05$ vs. group C, $^{b}p < 0.05$ vs. group N-1w(a), $^{c}p < 0.05$ vs. group N-2w(a), $^{b'}p < 0.05$ vs. group I-1w(a), $^{c'}p < 0.05$ vs. group I-2w(a), $^{*}p < 0.05$ vs. group I-1w(a), $^{\#}p < 0.05$ vs. group I-2w(a), $^{a'}p < 0.05$ vs. I-4w(a) group). (**D**) Expression of α-SMA, Collagen I, TGF-β1/Smad signaling pathway, and RhoA/ROCK signaling pathway of the joint capsule were examined by Western blotting. (**E-K**) The TGF-β1/GAPDH, α-SMA/GAPDH, Collagen I/GAPDH, p-Smad2/3/Smad2/3, ROCK1/GAPDH, total RhoA/GAPDH, and p-MLC/GAPDH of the joint capsule in each group. Data are expressed as mean ± standard deviation. ($^{a}p < 0.05$ vs. group C, $^{b}p < 0.05$ vs. group I-4w(b), $^{c}p < 0.05$ vs. N-4w(b), $^{*}p > 0.05$ vs. group C).

lease of joint immobilization does not completely reverse joint mobility restriction (Liu *et al*., 2022). Further studies have found that residual joint contractures after free movement are dominated by contractures of arthrogenic origin (Hu *et al*., 2023). Therefore, the application of new therapeutic strategies during immobilization is of great significance in improving joint contractures.

We evaluated arthrogenic mobility of the rat knee joint in the functional assessment of this study. We observed that the joint mobility of rats in group I(a) was less than that of rats in group C, which is consistent with the results of other studies in our group (Wang *et al*., 2023b). The joint capsule is an important component of the joint and is crucial for maintaining stability during joint movement (Wang *et al*., 2023a). Therefore, thickening of the joint capsule due to contracture can lead to reduced joint mobility. We observed that at the same time point during immobilization, knee mobility was higher in all N(a) groups than in the I(a) groups. Thus, nicorandil reduced the degree of capsular contracture caused by joint immobilization. In the histological evaluation, the results of Masson staining and immunohistochemistry for SMA further confirmed these functional

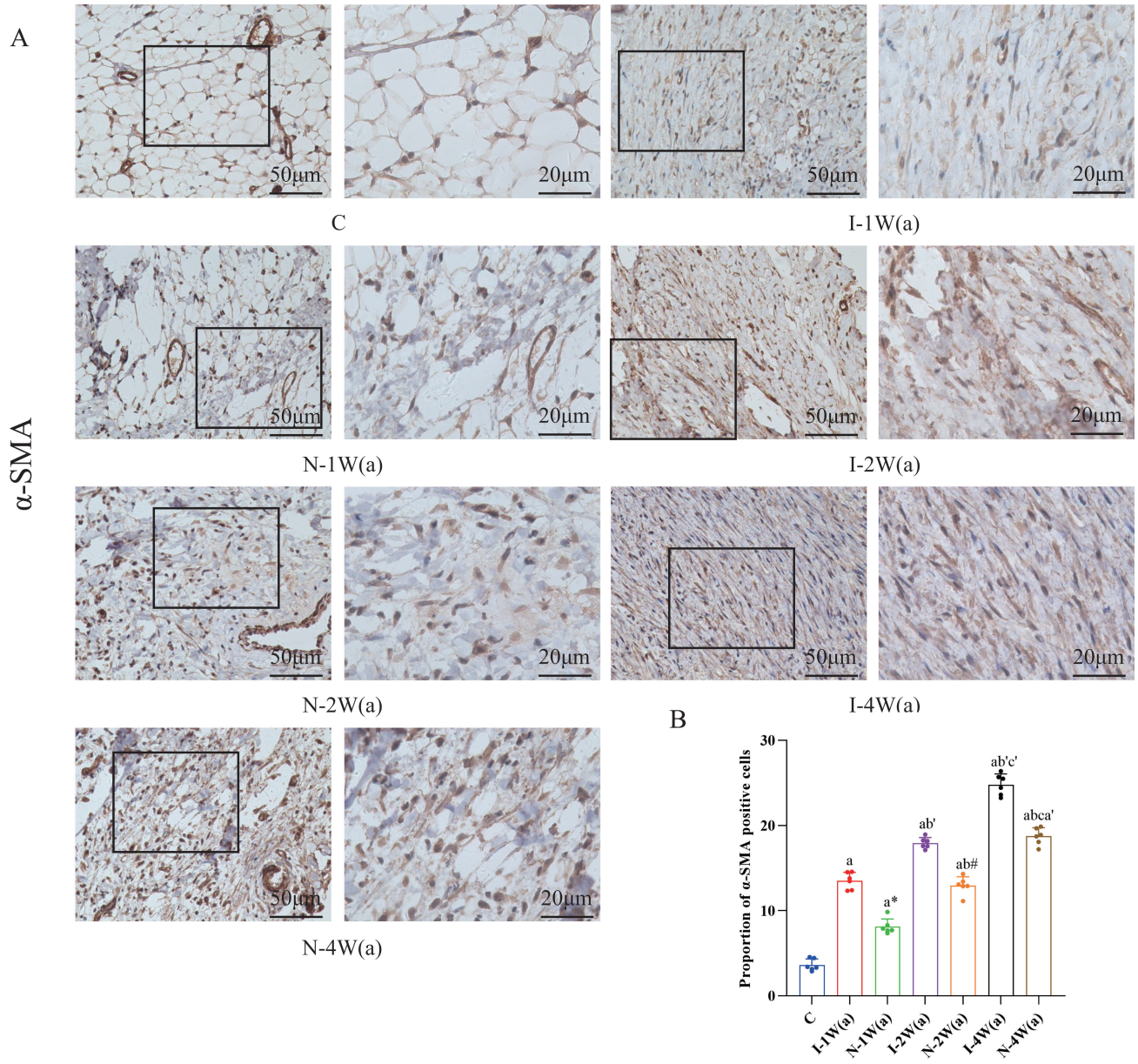

Fig. 6. Immunohistochemistry of α-SMA. (**A**) Immunohistochemical results of joint capsule α-SMA. The scale bars indicate 50 μm (left panels) and 20 μm (right panels). (**B**) Quantitative analysis of the percentage of α-SMA positive cells in each group. Data are expressed as mean ± standard deviation. ($^{a}p < 0.05$ vs. group C, $^{b}p < 0.05$ vs. group N-1w(a), $^{c}p < 0.05$ vs. group N-2w(a), $^{b'}p < 0.05$ vs. group I-1w(a), $^{c'}p < 0.05$ vs. group I-2w(a), $^{*}p < 0.05$ vs. group I-1w(a), $^{\#}p < 0.05$ vs. group I-2w(a), $^{a'}p < 0.05$ vs. I-4w(a) group).

results. Masson staining showed that the area of collagen fibers was larger in groups I(a) and N(a) than in group C. The collagen fiber area increased significantly over time in the I-2w(a) and I-4w(a) groups. However, after intervention treatment with nicorandil, the collagen fiber area in group N(a) was smaller than that in group I(a) at the same time point of immobilization. This suggests that nicorandil slows the development of fibrosis by inhibiting the excessive deposition of fibrous capsular connective tissue. This is consistent with the findings of Deng *et al.* (Deng *et al.*, 2022). As expected, histological assessment of α-SMA immunohistochemistry showed similar results. The proportion of α-SMA in group I(a) was significantly higher than that in group C and showed a time-dependent progression to 4 weeks after immobilization. After intervention with nicorandil, the proportion of α-SMA gradually decreased and reached its maximum at four weeks post-immobilization. This is in general agreement with the results of previous studies (Abdel-Aziz *et al.*, 2023; Abdel-Sattar *et al.*, 2020).

Nicorandil also has potent anti-inflammatory and antioxidant properties. As in a previously conducted study (Kseibati *et al.*, 2020), the levels of lymphocytes, neu-

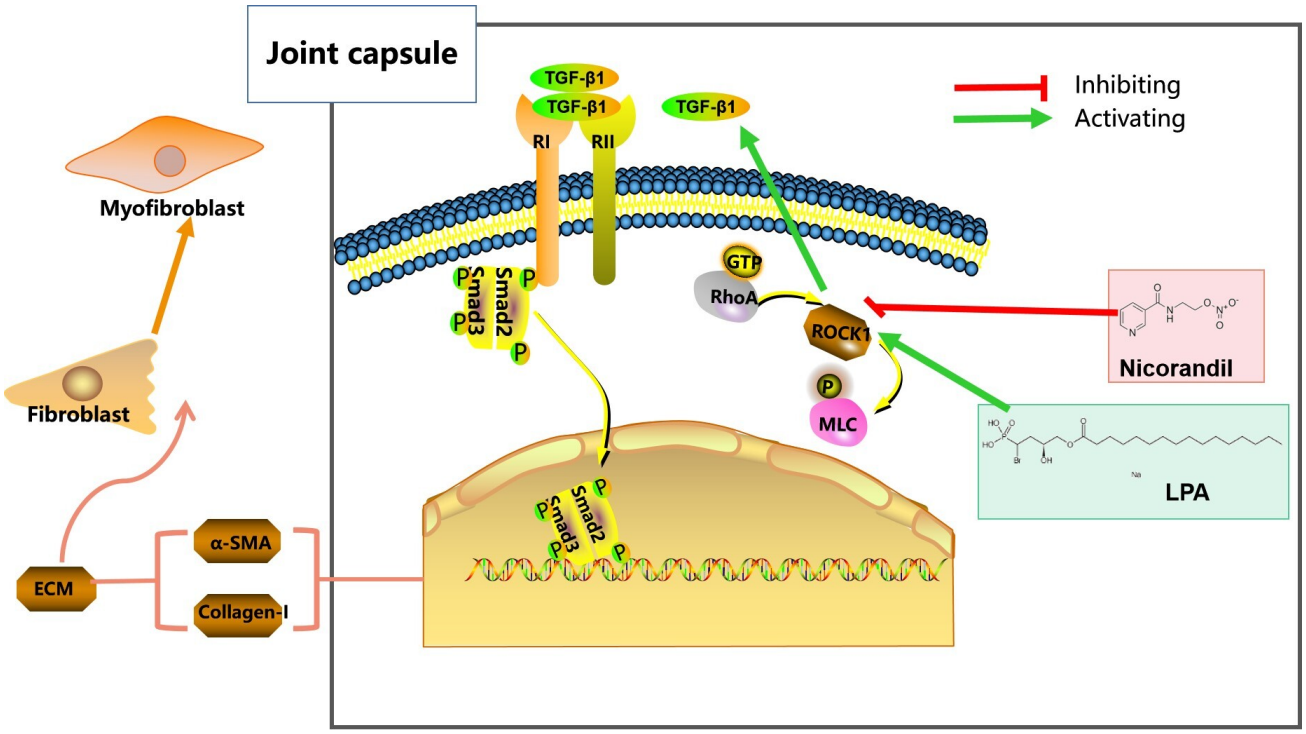

Fig. 7. Schematic diagram of nicorandil to attenuate immobilization-induced joint capsule fibrosis.

trophils, malondialdehyde (MDA), superoxide dismutase (SOD), and reduced glutathione (GSH) were significantly increased in the lung tissues of rats that had been orally administered bleomycin (BLM). Nicorandil significantly attenuated the activity of these compounds. In the unilateral ureteral obstruction (UUO) rat model of renal fibrosis, the levels of TNF-α and IL6 were significantly elevated in renal tissues. However, these levels were attenuated after treatment with nicorandil (Abdel-Aziz *et al*., 2023). In another study, silica was used to induce lung fibrosis in rats. They found that nicorandil effectively resolved oxidant/antioxidant disorders by downregulating iNOS (El-Kashef, 2018). We observed that the number of inflammatory cells was higher in rats in group I(a) than in those in group C, and nicorandil significantly attenuated the increase in inflammatory cells. Chronic inflammation in tissues ultimately leads to the proliferation and activation of fibroblasts into myofibroblasts, excessive deposition of collagen fibers, interstitial fibrosis, and the appearance of scar tissue (Della Latta *et al*., 2015).

Our results showed that TGF-β1/Smad pathway signaling was significantly enhanced in the articular capsule of the rat knee joint after immobilization. Activation of TGF-β1/Smad pathway signaling leads to fibrosis of the knee joint capsule. Nicorandil intervention reduced the activation of the above pathway. TGF-β1 is a cytokine that maintains homeostasis of the immune system. It is involved in coordinating tissue repair after tissue injury. When intracellular mechanical resistance is elevated to a certain level, TGF-β1 is further activated and promotes fibroblast activation in myofibroblasts (Lodyga and Hinz, 2020). Smad2/3 is a major downstream target. Smad signaling is a key mechanism involved in this process. The p-Smad2/3 complex enters the nucleus to regulate downstream proteins. Consistent with our expectations, we found that the levels of both TGF-β1 and p-Smad2/3 were elevated in I-4w(b) compared to those in Group C. After nicorandil treatment, TGF-β1 and p-Smad2/3 levels were significantly lower in group N-4w(b).

The integration of molecular signaling between TGF-β1/Smad and Rhoa/ROCK has been studied. Previous studies have found that TGF-β1 induces profound activation of RhoA, which further generates actin stress fibers and promotes α-SMA expression. Interestingly, the RhoA inhibitor Y27632 inhibited TGF-β-induced α-SMA expression but had no effect on Smad signaling (Sandbo *et al*., 2011). Li *et al*. (2021) found that TGF-β1 promotes migration and induces cytoskeletal remodeling of primary rat hepatic stellate cells (HSCs) through chemotaxis and haptotaxis mechanisms, which are based on the mechanism of increased RhoA activity (Li *et al*., 2012). TGF-β1 also regulates F-actin formation through RhoA/ROCK signaling. Inhibition of the RhoA signaling pathway with Y27632, a ROCK inhibitor, resulted in a significant decrease in the expression of α-SMA and Collagen I in TGF-β1-treated HSC-T6 cells (Moon *et al*., 2019). Downregulation of ROCK expression also reduces cardiac fibrosis (Sawada and Liao, 2014). The pharmacological effects of nicorandil may be mediated through RhoA/ROCK signaling. It has been demonstrated (Lee *et al*., 2017) that nicorandil

Fig. 8. Blood pressure measurement in rats.

stimulates macrophage differentiation toward the M2 phenotype through RhoA/ROCK signaling and ultimately attenuates cardiac fibrosis. Considering the involvement of RhoA/ROCK signaling, we evaluated the molecules in the RhoA/ROCK signaling pathway and their phosphorylation levels. In the present study, no significant difference in total RhoA levels was observed between the groups in test b. However, the protein levels of ROCK1 and p-MLC, the downstream products of the RhoA/ROCK pathway, were higher in group I-4w(b) than in group C, suggesting that RhoA/ROCK signaling was activated after immobilization, whereas the levels of ROCK1 and p-MLC were significantly lower in group N-4w(b) than in I-4w(b).

To further verify whether nicorandil exerted an antifibrotic effect through the RhoA/ROCK signaling pathway, we conducted additional experiments. In this trial, we treated rats with LPA (a ROCK activator), which effectively promoted RhoA/ROCK activation and reversed the antifibrotic effects of nicorandil. The protein expression level of the TGF-β1/Smad signaling pathway was inhibited to some extent in the N+LPA group compared with the I-4w(b) group. However, inhibition of the TGF-β1/Smad signaling pathway was much weaker in the N+LPA group than in the experimental group using nicorandil alone. Previous studies have demonstrated that nicorandil attenuates cardiac, pulmonary, hepatic, and renal fibrosis (Abdel-Sattar *et al*., 2020; Deng *et al*., 2022; Harb *et al*., 2021; Harb *et al*., 2023) by lowering TGF-β1 and/or inhibiting Smad2/3 phosphorylation. In N-4w(b), we found that various fibrosis indicators, such as collagen proliferation area, α-SMA, and TGF-β1, were significantly inhibited. After LPA intervention, all the above indicators were reversed to different degrees. However, we did not evaluate the expression levels of fibrosis-related genes due to the limitations of the experimental conditions.

It is necessary to acknowledge the limitations of this study. Before the experiment officially began, we allowed six normal rats to take nicorandil orally for up to 4 weeks, during which time there was no significant decrease in blood pressure (BP-2010A, Softron Biotechnology, Beijing, China) (Fig. 8). But we did not monitor blood pressure in immobilized rats. In addition, we did not test the bioavailability, pharmacokinetics, and toxicity of nicorandil. These will be the research directions of our team in the future. In subsequent studies, we will conduct further research on the above aspects.

Conclusion

In summary, treatment with nicorandil can significantly attenuate extension immobilization-induced arthrogenic fibrosis, and the mechanism may be related to RhoA/ROCK signaling-mediated inhibition of the TGF-β1/Smad signaling pathway. Therefore, in diseases requiring long-term joint immobilization, nicorandil may be used to prevent arthrofibrosis.

List of Abbreviations

LPA, lysophosphatidic acid; MRTF, Myocardin-Related Transcription Factor; SRF, serum response factor; ROM, range of motion; BCA, bicinchoninic acid; MDA, malondialdehyde; SOD, superoxide dismutase; GSH, glutathione; BLM, bleomycin; UUO, unilateral ureteral obstruction; HSCs, hepatic stellate cells.

Availability of Data and Materials

The datasets used and analyzed during the current study are available from the first author on reasonable request. All data generated or analyzed during this study are included in this published article. The manuscript, including related data, figures and tables have not been previously published and are not under consideration elsewhere.

Author Contributions

XML conceived the study, participated in its design and coordination, and drafted the manuscript. KW participated in the design, assisted with animal management, performed animal experiments, and helped draft the manuscript. ML performed animal experiments and molecular studies, and assisted with data statistics and analysis, participated in the drafting of the manuscript. QBZ performed the molecular studies, organized the data, and assisted in the drafting of the manuscript. YZ participated in the design and co-sequencing, and reviewed the final manuscript. All authors read and approved the final manuscript.

Ethics Approval and Consent to Participate

Animal care and experimental procedures were performed in accordance with the Guidelines for Animal Experimentation of Anhui Medical University and were approved by the Institutional Animal Care and Use Committee (LLSC20221126).

Acknowledgements

We thank Hua Wang from the Department of Toxicology, School of Public Health, Anhui Medical University for his valuable guidance and advice.

Funding

The Second Affiliated Hospital of Anhui Medical University (FY2021) Clinical Research Incubation Program (2021LCYB06); Clinical Medicine Discipline Construction Project of Anhui Medical University in 2022 (2022 lcxkEFY010); Health Research Program of Anhui (AHWJ2022b063; recipient: Yun Zhou); National Natural Science Incubation Program of the Second Hospital of Anhui Medical University (2022GMFY05; recipient: Yun Zhou); Summit Discipline Construction Project of Anhui Medical University (Clinical Medicine) in 2022 (2022GFXK-EFY08); Clinical Medicine Discipline Construction Project of Anhui Medical University in 2023 (2023lcxkEFY010).

Conflict of Interest

The authors declare no conflict of interest.

Appendix

See Fig. 8.

References

Abdel-Aziz HM, Ibrahem NE, Mekawy NH, Fawzy A, Mohamad NM, Samy W (2023) Nicorandil and bone marrow-derived mesenchymal stem cells therapeutic effect after ureteral obstruction in adult male albino rats. Current Molecular Pharmacology 16: 124-138. DOI: 10.2174/1874467215666220322113734.

Abdel-Sattar AR, Abo-Saif AA, Aboyoussef AM (2020) Nicorandil and atorvastatin attenuate carbon tetrachloride - induced liver fibrosis in rats. Immunopharmacology and Immunotoxicology 42: 582-593. DOI: 10.1080/08923973.2020.1830104.

Davies MR, Lee L, Feeley BT, Kim HT, Liu X (2017) Lysophosphatidic acid-induced RhoA signaling and prolonged macrophage infiltration worsens fibrosis and fatty infiltration following rotator cuff tears. Journal of Orthopaedic Research: Official Publication of the Orthopaedic Research Society 35: 1539-1547. DOI: 10.1002/jor.23384.

Della Latta V, Cecchettini A, Del Ry S, Morales MA (2015) Bleomycin in the setting of lung fibrosis induction: From biological mechanisms to counteractions. Pharmacological Research 97: 122-130. DOI: 10.1016/j.phrs.2015.04.012.

Deng HF, Zou J, Wang N, Ma H, Zhu LL, Liu K, Liu MD, Wang KK, Xiao XZ (2022) Nicorandil alleviates cardiac remodeling and dysfunction post -infarction by up-regulating the nucleolin/autophagy axis. Cellular Signalling 92: 110272. DOI: 10.1016/j.cellsig.2022.110272.

El-Kashef DH (2018) Nicorandil ameliorates pulmonary inflammation and fibrosis in a rat model of silicosis. International Immunopharmacology 64: 289-297. DOI: 10.1016/j.intimp.2018.09.017.

Garnier-Raveaud S, Faury G, Mazenot C, Cand F, Godin-Ribuot D, Verdetti J (2002) Highly protective effects of chronic oral administration of nicorandil on the heart of ageing rats. Clinical and Experimental Pharmacology & Physiology 29: 441-448. DOI: 10.1046/j.1440-1681.2002.03679.x.

Hanna M, Liu H, Amir J, Sun Y, Morris SW, Siddiqui MAQ, Lau LF, Chaqour B (2009) Mechanical regulation of the proangiogenic factor CCN1/CYR61 gene requires the combined activities of MRTF-A and CREB-binding protein histone acetyltransferase. The Journal of Biological Chemistry 284: 23125-23136. DOI: 10.1074/jbc.M109.019059.

Harb I, Ashour H, Rashed LA, Mostafa A, Samir M, Aboulhoda BE, El-Hanbuli H, Rashwan E, Mahmoud H (2023) Nicorandil mitigates amiodarone-induced pulmonary toxicity and fibrosis in association with the inhibition of lung TGF-β1/PI3K/Akt1-p/mTOR axis in rats. Clinical and Experimental Pharmacology & Physiology 50: 96-106. DOI: 10.1111/1440-1681.13728.

Harb IA, Ashour H, Sabry D, El-Yasergy DF, Hamza WM, Mostafa A (2021) Nicorandil prevents the nephrotoxic effect of cyclosporine-A in albino rats through modulation of HIF-1α/VEGF/eNOS signaling. Canadian Journal of Physiology and Pharmacology 99: 411-417. DOI: 10.1139/cjpp-2020-0012.

Hu C, Zhang QB, Wang F, Wang H, Zhou Y (2023) The effect of extracorporeal shock wave on joint capsule fibrosis in rats with knee extension contracture: a preliminary study. Connective Tissue Research 64: 469-478. DOI: 10.1080/03008207.2023.2217254.

Huang PP, Zhang QB, Zhou Y, Liu AY, Wang F, Xu QY, Yang F (2021) Effect of radial extracorporeal shock wave combined with ultrashort wave diathermy on fibrosis and contracture of muscle. American Journal of Physical Medicine & Rehabilitation 100: 643-650. DOI: 10.1097/PHM.0000000000001599.

Jiang C, Huang H, Liu J, Wang Y, Lu Z, Xu Z (2012) Fasudil, a Rho-kinase inhibitor, attenuates bleomycin-induced pulmonary fibrosis in mice. International Journal of Molecular Sciences 13: 8293-8307. DOI: 10.3390/ijms13078293.

Komers R (2013) Rho kinase inhibition in diabetic kidney disease. British Journal of Clinical Pharmacology 76: 551-559. DOI: 10.1111/bcp.12196.

Kseibati MO, Shehatou GSG, Sharawy MH, Eladl AE, Salem HA (2020) Nicorandil ameliorates bleomycin-induced pulmonary fibrosis in rats through modulating eNOS, iNOS, TXNIP and HIF-1α levels. Life Sciences 246: 117423. DOI: 10.1016/j.lfs.2020.117423.

Lee TM, Lin MS, Chang NC (2008) Effect of ATP-sensitive potassium channel agonists on ventricular remodeling in healed rat infarcts. Journal of the American College of Cardiology 51: 1309-1318. DOI: 10.1016/j.jacc.2007.11.067.

Lee TM, Lin SZ, Chang NC (2018) Nicorandil regulates the macrophage skewing and ameliorates myofibroblasts by inhibition of RhoA/Rho-kinase signalling in infarcted rats. Journal of Cellular and Molecular Medicine 22: 1056-1069. DOI: 10.1111/jcmm.13130.

Li J, Huang B, Dong L, Zhong Y, Huang Z (2021) WJ-MSCs intervention may relieve intrauterine adhesions in female rats via TGF-β1-mediated Rho/ROCK signaling inhibition. Molecular Medicine Reports 23: 8. DOI: 10.3892/mmr.2020.11646.

Li L, Wang JY, Yang CQ, Jiang W (2012) Effect of RhoA on transforming growth factor β1-induced rat hepatic stellate cell migration. Liver International 32: 1093-1102. DOI: 10.1111/j.1478-3231.2012.02809.x.

Liu AY, Zhang QB, Zhu HL, Xiong YW, Wang F, Huang PP, Xu QY, Zhong HZ, Wang H, Zhou Y (2022) Low-frequency electrical stimulation alleviates immobilization-evoked disuse muscle atrophy by repressing autophagy in skeletal muscle of rabbits. BMC Musculoskeletal Disorders 23: 398. DOI: 10.1186/s12891-022-05350-5.

Lodyga M, Hinz B (2020) TGF-β1 - A truly transforming growth factor in fibrosis and immunity. Seminars in Cell & Developmental Biology 101: 123-139. DOI: 10.1016/j.semcdb.2019.12.010.

Luchsinger LL, Patenaude CA, Smith BD, Layne MD (2011) Myocardin-related transcription factor-A complexes activate type I collagen expression in lung fibroblasts. The Journal of Biological Chemistry 286: 44116-44125. DOI: 10.1074/jbc.M111.276931.

Mack CP, Somlyo AV, Hautmann M, Somlyo AP, Owens GK (2001) Smooth muscle differentiation marker gene expression is regulated by RhoA-mediated actin polymerization. The Journal of Biological Chemistry 276: 341-347. DOI: 10.1074/jbc.M005505200.

Mohamed YS, Ahmed LA, Salem HA, Agha AM (2018) Role of nitric oxide and KATP channel in the protective effect mediated by nicorandil in bile duct ligation-induced liver fibrosis in rats. Biochemical Pharmacology 151: 135-142. DOI: 10.1016/j.bcp.2018.03.003.

Moon MY, Kim HJ, Kim MJ, Uhm S, Park JW, Suk KT, Park JB, Kim DJ, Kim SE (2019) Rap1 regulates hepatic stellate cell migration through the modulation of RhoA activity in response to TGF-β1. International Journal of Molecular Medicine 44: 491-502. DOI: 10.3892/ijmm.2019.4215.

Sandbo N, Lau A, Kach J, Ngam C, Yau D, Dulin NO (2011) Delayed stress fiber formation mediates pulmonary myofibroblast differentiation in response to TGF-β. American Journal of Physiology. Lung Cellular and Molecular Physiology 301: L656-66. DOI: 10.1152/ajplung.00166.2011.

Sawada N, Liao JK (2014) Rho/Rho-associated coiled-coil forming kinase pathway as therapeutic targets for statins in atherosclerosis. Antioxidants & Redox Signaling 20: 1251-1267. DOI: 10.1089/ars.2013.5524.

Shimizu T, Narang N, Chen P, Yu B, Knapp M, Janardanan J, Blair J, Liao JK (2017) Fibroblast deletion of ROCK2 attenuates cardiac hypertrophy, fibrosis, and diastolic dysfunction. JCI Insight 2: e93187. DOI: 10.1172/jci.insight.93187.

Sunamura S, Satoh K, Kurosawa R, Ohtsuki T, Kikuchi N, Elias-Al-Mamun M, Shimizu T, Ikeda S, Suzuki K, Satoh T, Omura J, Nogi M, Numano K, Siddique MAH, Miyata S, Miura M, Shimokawa H (2018) Different roles of myocardial ROCK1 and ROCK2 in cardiac dysfunction and postcapillary pulmonary hypertension in mice. Proceedings of the National Academy of Sciences

of the United States of America 115: E7129-E7138. DOI: 10.1073/pnas.1721298115.

Tsou PS, Haak AJ, Khanna D, Neubig RR (2014) Cellular mechanisms of tissue fibrosis. 8. Current and future drug targets in fibrosis: focus on Rho GTPase-regulated gene transcription. American Journal of Physiology. Cell Physiology 307: C2-C13. DOI: 10.1152/ajpcell.00060.2014.

Wang F, Wang H, Li M, Jia S, Wang J, Zhang J, Fan Y (2023a) The role of the joint capsule in the stability of the elbow joint. Medical & Biological Engineering & Computing 61: 1439-1448. DOI: 10.1007/s11517-023-02774-6.

Wang F, Zhou CX, Zheng Z, Li DJ, Li W, Zhou Y (2023b) Metformin reduces myogenic contracture and myofibrosis induced by rat knee joint immobilization via AMPK-mediated inhibition of TGF-β1/Smad signaling pathway. Connective Tissue Research 64: 26-39. DOI: 10.1080/03008207.2022.2088365.

Yu H, Zhu J, Chang L, Liang C, Li X, Wang W (2021) 3-Bromopyruvate decreased kidney fibrosis and fibroblast activation by suppressing aerobic glycolysis in unilateral ureteral obstruction mice model. Life Sciences 272: 119206. DOI: 10.1016/j.lfs.2021.119206.

Zhang R, Zhang QB, Zhou Y, Zhang R, Wang F (2023) Possible mechanism of static progressive stretching combined with extracorporeal shock wave therapy in reducing knee joint contracture in rats based on MAPK/ERK pathway. Biomolecules & Biomedicine 23: 277-286. DOI: 10.17305/bjbms.2022.8152.

Zhou CX, Wang F, Zhou Y, Fang QZ, Zhang QB (2023) Formation process of extension knee joint contracture following external immobilization in rats. World Journal of Orthopedics 14: 669-681. DOI: 10.5312/wjo.v14.i9.669.

Zhou Y, Little PJ, Xu S, Kamato D (2021) Curcumin inhibits lysophosphatidic acid mediated MCP-1 expression via blocking ROCK signalling. Molecules (Basel, Switzerland) 26: 2320. DOI: 10.3390/molecules26082320.

Editor's note: The Scientific Editor responsible for this paper was Denitsa Docheva.